CrossMark

Redistribution of soil organic matter by permafrost disturbance in the Canadian High Arctic

David M. Grewer · Melissa J. Lafrenière ·
Scott F. Lamoureux · Myrna J. Simpson

Abstract With increased warming in the Arctic, permafrost thaw may induce localized physical disturbance of slopes. These disturbances, referred to as active layer detachments (ALDs), redistribute soil across the landscape, potentially releasing previously unavailable carbon (C). In 2007–2008, widespread ALD activity was reported at the Cape Bounty Arctic Watershed Observatory in Nunavut, Canada. Our study investigated organic matter (OM) composition in soil profiles from ALD-impacted and undisturbed areas. Solid-state ^{13}C nuclear magnetic resonance (NMR) and solvent-extractable biomarkers were used to characterize soil OM. Throughout the disturbed upslope profile, where surface soils and vegetation had been removed, NMR revealed low O-alkyl C content and biomarker analysis revealed low concentrations of solvent-extractable compounds suggesting enhanced erosion of labile-rich OM by the ALD. In the disturbed downslope region, vegetation remained intact but displaced material from upslope produced lateral compression ridges at the surface. High O-alkyl content in the surface horizon was consistent with enrichment of carbohydrates and peptides, but low concentrations of labile biomarkers (i.e., sugars) suggested the presence of relatively unaltered labile-rich OM. Decreased O-alkyl content and biomarker concentrations below the surface contrasted with the undisturbed profile and may indicate the loss of well-established pre-ALD surface drainage with compression ridge formation. However, pre-ALD profile composition remains unknown and the observed decreases may result from nominal pre-ALD OM inputs. These results are the first to establish OM composition in ALD-impacted soil profiles, suggesting reallocation of permafrost-derived soil C to areas where degradation or erosion may contribute to increased C losses from disturbed Arctic soils.

D. M. Grewer · M. J. Simpson
Department of Chemistry, University of Toronto, 80 St George St, Toronto, ON M5S 3H6, Canada

D. M. Grewer · M. J. Simpson (✉)
Department of Physical and Environmental Sciences, University of Toronto, 1265 Military Trail, Toronto, ON M1C 1A4, Canada
e-mail: myrna.simpson@utoronto.ca

M. J. Lafrenière · S. F. Lamoureux
Department of Geography and Planning, Queen's University, 99 University Ave., Kingston, ON K7L 3N6, Canada

Introduction

Soils in permafrost regions, such as those in the Canadian high Arctic, are estimated to contain nearly half of the global reservoirs of carbon (C) stored belowground (Schuur et al. 2009; Tarnocai et al. 2009). Recent warming in high latitudes has threatened the stability of C in northern permafrost regions with a changing climate (Vonk and Gustafsson 2013). Consequently, current projections have proposed a positive climate feedback of C release from terrestrial Arctic ecosystems to the atmosphere resulting from increased thaw and subsequent microbial respiration of C in high latitude permafrost soils (Davidson and Janssens 2006; Zimov et al. 2006a; Schuur et al. 2009; Schaefer et al. 2011; Koven et al. 2011; MacDougall et al. 2012). Short growing seasons in the Arctic can limit ecosystem primary production and low soil temperatures typically restrict biogeochemical cycling. Accumulation of organic matter (OM) in Arctic soils may be enhanced over successive cycles through preservation of detritus within the perennially frozen ground (Hobbie et al. 2002; Mikan et al. 2002; Sjögersten et al. 2003). In addition, cryoturbation in permafrost can bury accumulated C belowground (Bockheim and Tarnocai 1998). Over time, permafrost soils can accumulate relatively large amounts of OM, which may become more vulnerable to decomposition upon thawing (Nowinski et al. 2008; Hartley et al. 2010). Recent studies have shown that the OM composition of deeper Arctic soils may contain a substantial labile component via long-term preservation in permafrost (Waldrop et al. 2010; Vonk and Gustafsson 2013; Ewing et al. 2015a, b). With increased vulnerability of aged labile C stocks to degradation, the release of permafrost-derived OM may increase CO_2 flux to the atmosphere via microbial respiration (Drake et al. 2015; Ewing et al. 2015a; Mann et al. 2015). Enhanced warming conditions may therefore increase availability of this previously inaccessible C from receding permafrost and further intensify the ecosystem response to climate change (MacDougall et al. 2012; Natali et al. 2014).

Accelerated OM degradation in a warmer climate may also be stimulated by localized physical disruptions within Arctic soils (Pautler et al. 2010a, b; Woods et al. 2011; Lamoureux and Lafrenière 2014; Louiseize et al. 2014; Grewer et al. 2015). Persistent above freezing temperatures during the spring and summer months typically thaw the upper 40-100 cm of the soil in continuous permafrost regions and generate an active layer where the biogeochemical cycling of C occurs (Davis 2001). Under enhanced warming conditions, thawing may increase active layer thickness beyond the typical frost table depth. On sloped terrain, saturation of soil overburden during snow melt and rainfall events can decrease overall shear strength and destabilize the thickening active layer (Lewis et al. 2005; Lamoureux and Lafrenière 2009). This instability can initiate events referred to as active layer detachments (ALDs), which can transfer surface material hundreds of meters downslope across the frozen base layer (Lewis et al. 2005; Lewkowicz and Harris 2005a; Lewkowicz 2007). Though data is limited, the frequency of large scale detachments has been reported to have increased in recent years across the high Arctic and may indicate an increasingly unstable landscape resulting from a warming climate and permafrost degradation (Lewkowicz and Harris 2005b; Jorgenson et al. 2006; Bowden et al. 2008; Lantz and Kokelj 2008; Lamoureux and Lafrenière 2009). The upslope region of an ALD-impacted area may be stripped of the soil active layer and vegetation, leaving behind a barren scar zone comprised of the underlying mineral soil formerly at or below the permafrost transition layer. This deeper soil layer uncovered upslope potentially contains older, labile-rich OM, which had accumulated prior to ALD activity. Exposure of previously buried labile OM may stimulate microbial activity and further enhance degradation of stored soil C (Pautler et al. 2010a). Moreover, the redistribution of soil OM shifted downslope may promote enhanced erosion and degradation during transport, further contributing to potential C losses from ALDs. The surge of labile OM may also encourage priming of the soil which results from an increase in microbial activity from the added labile inputs, facilitating enhanced decomposition of native soil OM and ultimately contributing to increased CO_2 flux in Arctic ecosystems (Kuzyakov 2002; Fontaine et al. 2004; Hartley et al. 2010).

To investigate the impact of ALDs to High Arctic soils, Pautler et al. (2010a) examined surface soils from both disturbed and undisturbed areas with results generally indicating increased labile C in soils recently disturbed by ALDs. However, the subsurface soils and soils exposed within the upslope scar zone of the

disturbances remain unstudied. The current study compares and contrasts soil OM composition from depth profiles in ALD-impacted areas with those from an undisturbed site. One undisturbed soil profile and two separate profiles where widespread ALD activity was reported in 2007 and 2008 from the Cape Bounty Arctic Watershed Observatory (CBAWO), Nunavut, Canada (74°50′N, 109°30′W) were collected (Fig. 1). One of the disturbed profiles was located near the centre of the scar zone while the second profile was sampled downslope within the lateral compression ridges which commonly occur in the material accumulation region of elongated forms of ALDs (Lamoureux and Lafrenière 2009). We hypothesized that the removal of the overlying soils by ALDs would expose and redistribute previously buried permafrost resulting in molecular-level compositional differences between the disturbed upslope and downslope areas as well as the undisturbed region. Additionally, with increased labile C reported in fluvial sediment downstream of the disturbance (Grewer et al. 2015), we examined the soil profiles for evidence of enrichment in labile C potentially resulting from long-term preservation below ground. Gas chromatography-mass spectrometry (GC–MS) was used to characterize solvent extractable compounds isolated from the soils (Otto and Simpson 2005). Solid-state cross polarization magic angle spinning (CPMAS) ^{13}C nuclear magnetic resonance (NMR) spectroscopy was also performed to obtain general structural information with respect to overall soil OM composition (Kögel-Knabner 1997; Simpson et al. 2008). This study thus reports changes to OM composition in Arctic soil after the redistribution of material via ALDs which may subsequently impact biogeochemical cycling in the High Arctic.

Materials and methods

Study location

The landscape at the CBAWO is largely composed of a thin layer of unconsolidated glacial sediment and Holocene marine deposits overlying bedrock primarily composed of Hecla Bay Formation sandstones and siltstones (Hodgson et al. 1984). Soils are characterized by shallow organic horizons (<10 cm) with low organic carbon (OC) content (1–3 %) and developed from largely unaltered parent material (Lamoureux

et al. 2014). Permafrost in the region is continuous with active layer thickness typically varying between 50 and 100 cm (Lamoureux et al. 2009; Lewis et al. 2012). Surface topography is characterized by gently sloping terrain with shallow channelized drainage. Intermittent gullies create depressions in the landscape, which preferentially accumulate wind-blown snow and exhibit diffuse flow drainage patterns (Lamoureux and Lafrenière 2009). Sparse polar desert tundra vegetation is dominated by mosses and prostrate dwarf shrub graminoids (Walker et al. 2005). The Ptarmigan region of the CBAWO West River catchment, which underwent slope failure due to ALD activity in 2007/2008, exhibits concave depressions downslope, which are vulnerable to snowpack accumulation and subsequent seasonal runoff enhancement. In addition, the pre-ALD landscape of Ptarmigan demonstrated well-established channelization supporting efficient drainage while post-disturbance conditions supported enhanced channel incision (Lamoureux et al. 2014).

The disturbance at Ptarmigan demonstrated an elongated form of ALD morphology (Lewkowicz and Harris 2005a) and covered approximately 10.8 % of the total area of the subcatchment spanning 350 m along the pre-existing channel (Lamoureux et al. 2014). Downslope movement of material left behind a scar zone in the upslope region, exposing occasional ground ice and clay slurries, which were ejected downslope during the year of the disturbance. The landscape was moderately fractured but much of the displaced vegetated surface soil remained intact (Lamoureux and Lafrenière 2009). Additionally, downslope movement inhibited by slope topography led to the formation of lateral compression ridges at the surface of soils within the slump region potentially constraining any enhanced erosion. Sustained sediment export attributed to erosion of ALD-impacted soils in the Ptarmigan region was reported in the channel for 5 years following the disturbance (Lamoureux et al. 2014).

Soil from the CBAWO was sampled in late July of 2012 at three locations (Fig. 1) selected to examine differences between undisturbed soil, the upslope scar zone and the downslope soil within the disturbed Ptarmigan region. The landscape in the Upper Goose region (UG) shared similar size, hydrology, geology, slope, soil, and vegetation cover as the Ptarmigan region while showing no sign of prior disturbance at the time of sampling. However, variation in OM composition potentially exists between upslope and

Fig. 1 Map of the West River catchment, Cape Bounty Arctic Watershed Observatory with soil profile sample locations. Relative elevation is represented by 10 m contour intervals
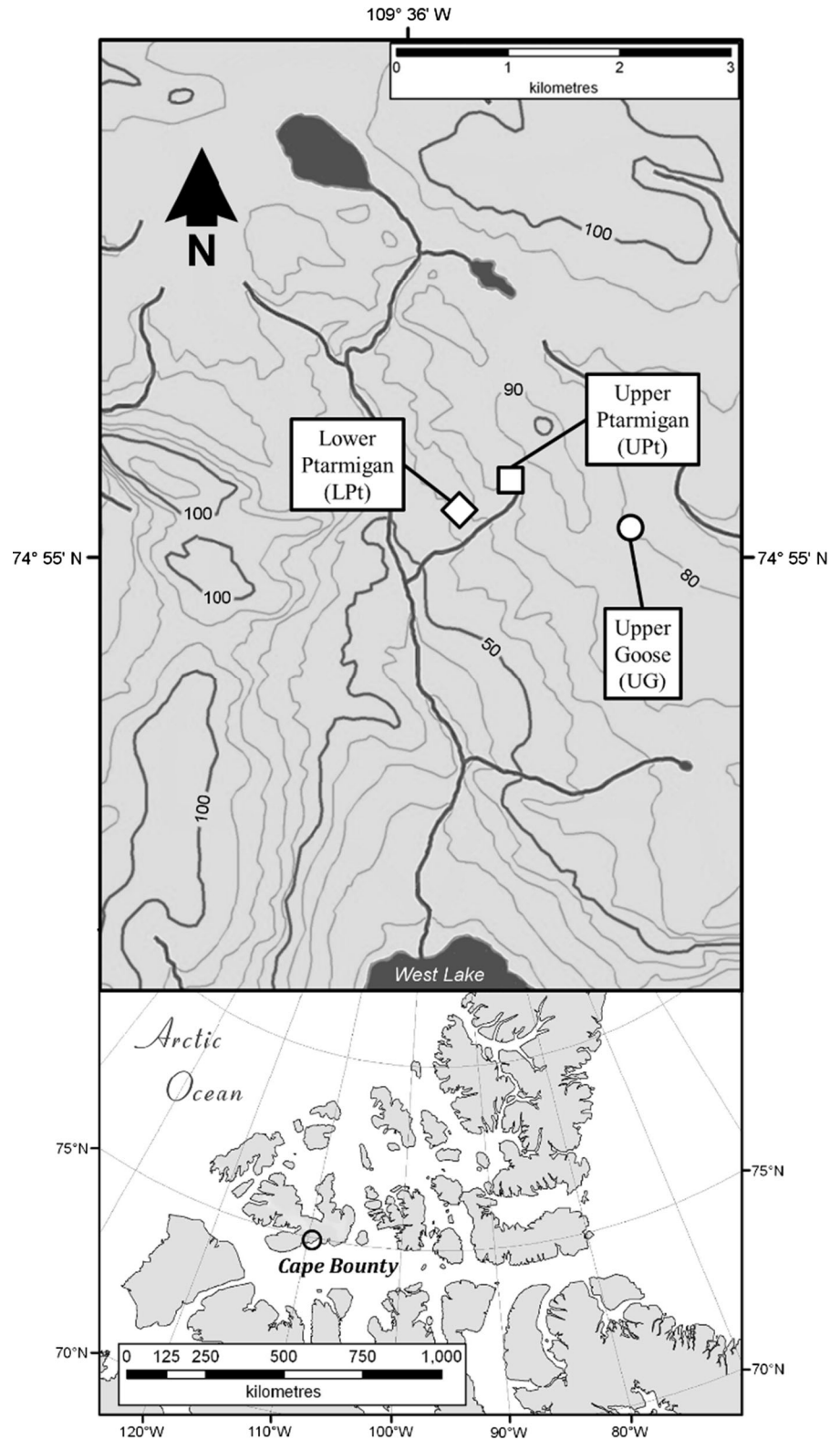
downslope soils within the undisturbed UG region and limits direct comparisons with the disturbed soils. Hence, within the scope of our current investigation and experimental framework, the undisturbed UG profile was considered as a relative reference point for comparisons to disturbed sites. The Upper Ptarmigan site (UPt) was situated upslope within the ALD scar zone where most of the active layer and vegetation was stripped away by the 2007–2008 ALD activity. At the time of sampling, recolonization by vegetation was not observed and the site remained bare (Fig. S1-A). At the Lower Ptarmigan site (LPt), sampled downslope within the ALD slump zone, much of the vegetation and soil was left intact. However, moderate surface disturbance caused by the sliding active layer soils from upslope produced lateral compression ridges at the surface of the LPt area (Fig. S1-B).

At each site, unfrozen soil samples for each profile were collected incrementally from the partially thawed active layer. Samples were collected at six depths: 0, 5, 15, 30, 40 cm, and maximum depths which were 65, 70, or 90 for UG, UPt, and LPt respectively. The variation in depth of the lower portions of each profile was due to differences in the depth of the frost table at each site. After sampling, soil samples were frozen and stored at $-20\ ^\circ C$, then freeze-dried and ground with a clean mortar and pestle prior to analyses.

Organic carbon (OC) and nitrogen (N) content

Determination of OC was performed via combustion analysis of total C (Nelson and Sommers 1996) at 1350 °C in a stream of purified O_2 using the LECO SC-444 analyzer equipped with infrared detection (University of Guelph Agriculture and Food Laboratory, Ontario, Canada). Prior to combustion analysis, inorganic C content was removed by ashing samples 3 h at 475 °C (Nelson and Sommers 1996). This technique ensures the elimination of carbonates in the determination of OC without any interference from other conventional techniques requiring chemical pretreatment of the sample to determine inorganic C content (Johns et al. 2015). Analysis revealed no traces of inorganic C, therefore OC content was equivalent to total C. A minimum of 0.25 g of sample was used for each total C measurement (detection limit of 0.1 %). Expanded uncertainty of the LECO SC-444 analyzer for total C in soil was 8 % of the result.

Determination of total N content was performed using the Dumas method (Rutherford et al. 2008) on separate portions of each sediment sample (University of Guelph Agriculture and Food Laboratory, Ontario, Canada). Briefly, dry combustion of samples was performed in a sealed system wherein a stream of pure O_2 oxidized N compounds which were then converted to N_2 through a reduction furnace. Detection of reduced N was performed with a thermal conductivity cell on the LECO FP428 N analyzer. Approximately 0.20 g of each sample was used for total N (detection limit of 0.05 %). Expanded uncertainty of the LECO SC-444 analyzer for total N in soil was 24 % of the result.

Solid-state CPMAS ^{13}C NMR

Ground soil samples ($\sim$10–15 g) were pretreated with hydrofluoric acid (HF, 10 % v/v) to remove any paramagnetic minerals and concentrate OM prior to solid-state NMR analysis (Rumpel et al. 2006). Each soil sample was mixed with 200 mL HF solution and sealed in 250 mL Nalgene centrifuge bottles then agitated overnight. The supernatant HF solution was removed after centrifugation (5000 rpm for 10 min) and replaced with fresh HF daily for a total of 12 times. Samples were then rinsed 10 times with deionized water to remove excess salts and then freeze-dried and ground. About 100 mg of the freeze-dried sample was packed into a 4 mm zirconium rotor for NMR analysis. NMR spectra were obtained using a 500 MHz Bruker BioSpin Avance III spectrometer equipped with a 4 mm H–X MAS probe. Acquisition entailed a ramp-CP program and a MAS spinning rate of 13 kHz using contact time of 1 ms and a 1 s recycle delay (Conte et al. 2004). Four chemical shift regions corresponding to C functionality (Preston et al. 1997; Simpson et al. 2008) were integrated and normalized to the total C signal: alkyl C (0–50 ppm), O-alkyl C (50–110 ppm), aromatic C (110–165 ppm), and carbonyl C (165–215 ppm). The associated uncertainty of the whole spectrum using this method is reported to be ± 5 % of the total intensity (Dria et al. 2002).

Biomarker analysis by GC–MS

Solvent extractable biomarkers were isolated following the procedure of Otto and Simpson (2005) via sonication of the soil ($\sim$4 g) sequentially with 30 mL

each of three solvents: dichloromethane, dichloromethane/methanol (1:1 v/v), and methanol. The solvent extracts were combined and then filtered through glass fiber filters (Whatman GF/A and GF/F), concentrated via rotary evaporation, transferred into 2 mL glass vials and dried under a stream of N_2 prior to derivatization. All extractions were performed in triplicate and reported as means with corresponding standard errors.

Solvent extracts were derivatized prior to GC–MS analysis. Reactive functional groups (alcohols and carboxylic acids) were converted to trimethylsilyl ethers by adding 90 μL N,O-bis-(trimethylsilyl)trifluoroacetamide (BSTFA) and 10 μL anhydrous pyridine to each vial and heating for 1 h at 70 °C. After cooling, 400 μL hexane was added to each vial. The derivatized extracts were analyzed by GC–MS using an Agilent 6890 N GC coupled to an Agilent 5973 N quadrupole mass selective detector. Samples were injected (1 μL) using an Agilent 7683 autosampler with a 2:1 split ratio and inlet temperature of 280 °C. The GC was equipped with a HP-5MS fused silica capillary column (30 m × 0.25 mm id and 0.25 μm film thickness). The GC parameters were set as follows: initial oven temperature of 65 °C held for 2 min, temperature ramping from 6 to 300 °C at a rate of 6 °C/min and held for 20 min at the final temperature of 300 °C. Electron impact ionization (70 eV) was used and the mass spectrometer was operated in total ion current mode which scanned m/z from 50 to 650 Da. Biomarker quantification was performed with external standards which were representative of different OM constituents (*n*-tetracosane, methyl tricosanoate, *n*-docosanol and ergosterol). Agilent Chemstation G1701EA software was used to process GC–MS data and biomarkers were identified by interpretation of mass fragmentation patterns, comparison with MS libraries (Wiley 9th with NIST 2008) and analytical standards. Biomarker concentrations were normalized to OC content of each sample to facilitate comparisons between soil samples.

Results

Organic carbon (OC) and total nitrogen (N)

The undisturbed soil (UG) contained more OC at the surface (2.69 %, 0 cm), which decreased progressively with depth (Table 1). The disturbed upslope site (UPt) exhibited consistently low OC content throughout the soil profile (0.60–0.80 %). At disturbed downslope site (LPt), high surface OC (3.86 %, 0 cm) contrasted with lower concentrations in subsurface samples (0.68–0.80 %, 5–40 cm) but increased OC was observed at the maximum depth sampled (1.06 %, 90 cm).

Total N content (Table 1) in the undisturbed UG surface soil was 0.18 % and decreased progressively with depth (0.14–0.08 %) to the deepest sample (65 cm) where N was below detectable limits (<0.05 %). At the disturbed UPt site, total N was below detectable limits throughout most of the soil profile except for three mid-depth samples where N content was measured between 0.05 and 0.06 %. Throughout the disturbed LPt profile similarly low levels of N were measured (0.05–0.08 %) except in the surface soil where N content was 0.27 %.

Solid-state CPMAS ^{13}C NMR

The solid-state CPMAS ^{13}C NMR spectra (Fig. 2) and the integrated regions of interest (Table 2) provide general information regarding the overall C content of the soil. However, because this method is considered semi-quantitative, relative comparison between samples must be examined in conjunction with more quantitative data such as biomarker analysis (Preston 2014). The undisturbed profile at UG, provides a reference of what would typically be observed in undisturbed Arctic soils at Cape Bounty demonstrating relatively high levels of O-alkyl C (54 %) observed at the surface with lower aromatic C (10 %) and alkyl C (28 %) contributions. More intense signals within the O-alkyl region are generally consistent with labile-rich C structures such as sugars or peptides as well as methoxyl C, ethers, and wax esters resulting from the deposition of fresh plant detritus and microbial biomass (Baldock and Preston 1995; Amelung et al. 2008). The anomeric C peak in the O-alkyl region at 105 ppm also suggests the presence of carbohydrates (Preston et al. 1997). At UG, the O-alkyl signal decreased steadily with depth and at 65 cm the ^{13}C NMR spectrum was dominated by aromatic (47 %) and alkyl (42 %) moieties. Such changes are consistent with progressive biodegradation and an enrichment of more recalcitrant-rich C (Baldock and Preston 1995; Kögel-Knabner 1997). A

Table 1 Organic carbon (OC) content and total nitrogen (N) content in soil depth profile samples from the Cape Bounty Arctic Watershed Observatory

Sample site	Depth (cm)	OC (%)[†]	Total N (%)[††]
Upper Goose (UG)	0	2.69	0.18
	5	1.61	0.14
	15	1.21	0.11
	30	0.94	0.08
	40	0.92	0.08
	65	0.48	bdl[a]
Upper Ptarmigan (UPt)	0	0.71	bdl[a]
	5	0.78	bdl[a]
	15	0.79	0.05
	30	0.79	0.06
	40	0.80	0.06
	70	0.60	bdl[a]
Lower Ptarmigan (LPt)	0	3.86	0.27
	5	0.80	0.07
	15	0.78	0.06
	30	0.74	0.06
	40	0.68	0.05
	90	1.06	0.08

[a] *bdl* below detection limit, <0.05 %

[†] Expanded uncertainty (coverage factor of 95 %) for total carbon in soil: 8 % of the result

[††] Expanded uncertainty (coverage factor of 95 %) for total nitrogen in soil: 24 % of the result
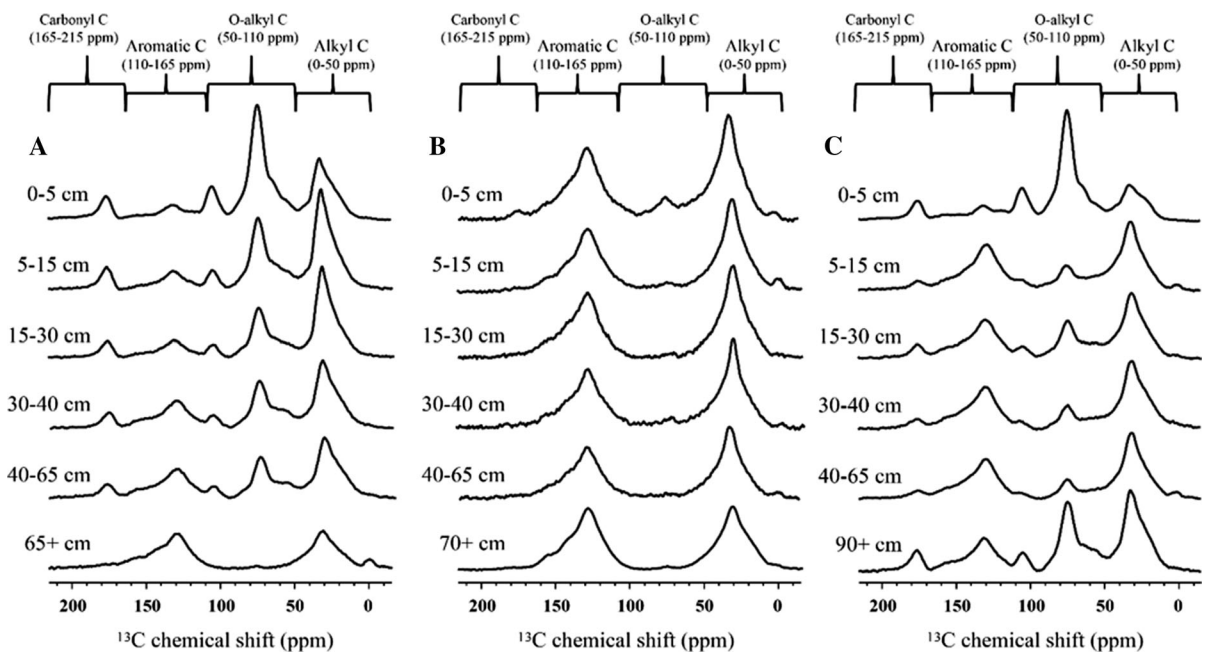
Fig. 2 Solid-state ^{13}C NMR spectra of soil depth profile samples from: **a** the undisturbed profile at Upper Goose (UG), **b** the disturbed profile at Upper Ptarmigan (UPt), and **c** the disturbed profile at Lower Ptarmigan (LPt) of the Cape Bounty Arctic Watershed Observatory

ratio of alkyl to O-alkyl C is commonly used to assess the relative level of OM decomposition as this ratio increases with progressive degradation (Baldock and Preston 1995; Sjögersten et al. 2003). The alkyl/O-alkyl ratios from UG (Table 2) were indicative of progressive degradation with depth, increasing

Table 2 Integrated contributions of four primary functional groups and alkyl/O-alkyl proxy elucidated from solid-state ^{13}C NMR results of three soil profiles from the Cape Bounty Arctic Watershed Observatory (values expressed as percent of total NMR signal from 0–215 ppm)

Sample site	Depth (cm)	Alkyl (0–50 ppm)	O-Alkyl (50–110 ppm)	Aromatic (110–165 ppm)	Carbonyl (165–215 ppm)	Alkyl/ O-alkyl
Upper Goose (UG)	0	28	54	10	8	0.52
	5	43	37	12	8	1.16
	15	47	32	14	7	1.47
	30	39	30	23	8	1.30
	40	39	28	26	7	1.39
	65	42	5	47	6	8.40
Upper Ptarmigan (UPt)	0	42	17	38	3	2.47
	5	45	13	40	2	3.46
	15	48	5	45	2	9.60
	30	44	13	41	2	3.38
	40	45	10	42	3	4.50
	70	43	7	48	2	6.14
Lower Ptarmigan (LPt)	0	22	58	13	7	0.38
	5	40	20	35	5	2.00
	15	38	26	30	6	1.46
	30	43	17	34	6	2.53
	40	45	15	35	5	3.00
	90	37	34	21	8	1.09

steadily from 0.52 at the surface to 1.39 in the 40 cm sample. A substantial increase in the alkyl/O-alkyl ratio was observed in the deepest soil at UG (8.40, 65 cm) suggesting highly degraded material.

Throughout the disturbed UPt profile, samples were dominated by aromatic (38–48 %) and alkyl (42–48 %) moieties with small contributions from O-alkyl C throughout the profile ranging from 5–17 %. Alkyl/O-alkyl ratios throughout UPt varied between 2.47 and 9.60 (Table 2) indicative of enhanced degradation relative to undisturbed UG soil. In addition, the UPt spectra were generally similar to the deepest soil at UG (65 cm) exhibiting aromatic C and alkyl C dominance (Table 2). This suggests the presence of recalcitrant-rich material, such as plant waxes or altered lignin (Baldock and Preston 1995; Preston et al. 1997), which are likely remnants of plant-derived detritus buried and degraded over time. This also indicates that the soil from the disturbed UPt scar zone may have originally been a deeper component of the profile prior to disturbance supporting the hypothesis that the ALD shifted much of the upper soil horizons away from UPt, thus exposing a much deeper mineral soil to the surface.

Downslope in the disturbed LPt profile, the surface soil produced a ^{13}C NMR spectrum similar to that of the UG surface soil with high levels of O-alkyl C (58 %), likely corresponding to greater labile C content from unaltered plant material. Moreover, the alkyl/O-alkyl ratio from the LPt surface soil exhibited the lowest value from the study (0.38, Table 2), which further indicates generally high levels of labile C and limited decomposition. However, immediately below the surface, O-alkyl content decreased substantially (20 %, 5 cm) and remained near this level (15–26 %) in the subsurface samples of the LPt soil profile (15–40 cm). Alkyl/O-alkyl ratios corroborate this decline in labile C below the surface (1.46–3.00 for subsurface samples: 5–40 cm, Table 2). At the maximum sampling depth in the LPt profile (90 cm), high O-alkyl C (34 %) relative to the overlying horizons and a decrease in the alkyl/O-alkyl ratio (1.09) suggested enrichment of labile C.

Total solvent extraction

The homologous series of each aliphatic lipid class (n-alkanes, n-alkanols, and n-alkanoic acids) were dominated by long-chain ($>C_{20}$) compounds at all sites (Fig. 3), which is indicative of vascular plant-derived sources (Amelung et al. 2008). A comprehensive summary of the biomarker data for each profile is listed in Tables S1–S3. In the undisturbed soil (UG), total n-alkane concentrations (Fig. 3) increased with depth in the top 30 cm of the soil profile (0.289 ± 0.008 to 0.439 ± 0.034 mg/g OC); then progressively decreased (0.310 ± 0.016 to 0.062 ± 0.006 mg/g OC). Similarly, the long-chain n-alkanol concentrations (Fig. 3) increased with depth through the upper 30 cm (1.722 ± 0.082 to 2.030 ± 0.228 mg/g OC) but then decreased with depth (1.068 ± 0.096 to 0.061 ± 0.006 mg/g OC). However, the distribution of n-alkanoic acids in the undisturbed UG profile (Fig. S4) was marked by the presence of short-chain n-alkanoic acids (0.158 ± 0.018 to 0.414 ± 0.070 mg/g OC, Fig. 4), mostly in the form of the C_{16} and C_{18} acids. The short-chain C_{16} and C_{18} acids can originate from both plant and microbial sources (Harwood and Russell 1984; Dinel et al. 1990). Still, long-chain acids ($>C_{20}$) were dominant with increasing concentrations through the upper 30 cm (1.387 ± 0.052 to 1.828 ± 0.183 mg/g OC) and progressive decline deeper in the soil

(0.443 ± 0.031 to 0.042 ± 0.004 mg/g OC). In contrast, the disturbed upslope soil (UPt) contained low concentrations of long-chain n-alkanes (0.068 ± 0.006 to 0.198 ± 0.012 mg/g OC) throughout the profile. However, small amounts of short-chain n-alkanes were observed in the disturbed UPt soil profile and may be suggestive of small concentrations of microbial sources (0.0032 ± 0.0002 to 0.0081 ± 0.0003 mg/g OC, Fig. 4). Low concentrations of n-alkanols at UPt (0.033 ± 0.002 to 0.128 ± 0.008 mg/g OC) were consistent throughout the profile (Fig. 3). Conversely, the n-alkanoic acid distribution at the disturbed UPt site (Figs. 4 and S2) was dominated by the short-chain C_{16} and C_{18} acids with much higher concentrations occurring 15+ cm below the surface (0.072 ± 0.005 to 0.311 ± 0.034 mg/g OC, Fig. 4) and lower concentrations of the long-chain homologues throughout the profile (0.023 ± 0.002 to 0.071 ± 0.006 mg/g OC, Fig. 3). At the disturbed downslope site (LPt), high concentrations of long-chain n-alkanes were observed in the surface sample (0 cm, 0.488 ± 0.022 mg/g OC) and at maximum depth (90 cm, 0.416 ± 0.024 mg/g OC) while concentrations in subsurface samples (5–40 cm) were lower (0.212 ± 0.011 to 0.256 ± 0.018 mg/g OC). Higher n-alkanol concentrations in the disturbed LPt profile were also observed in both the surface soil and the deepest point of the profile (0.560 ± 0.022 and 0.753 ± 0.017 mg/g OC
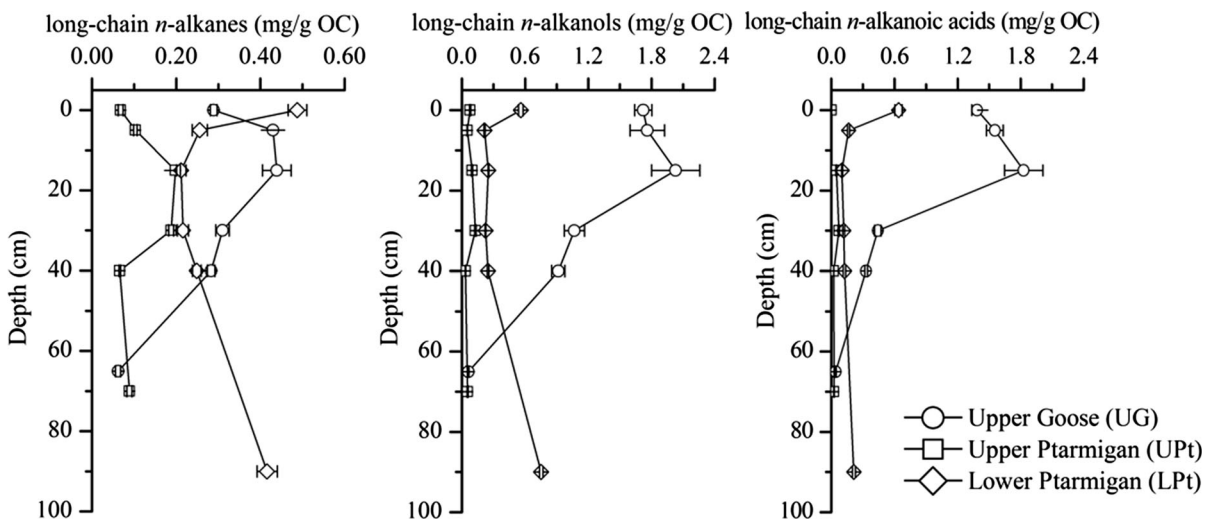
Fig. 3 Concentration of long-chain ($\geq C_{20}$) acyclic aliphatic lipid concentrations in the soil depth profiles at Cape Bounty. *Error bars* indicate standard error calculated from triplicate analysis
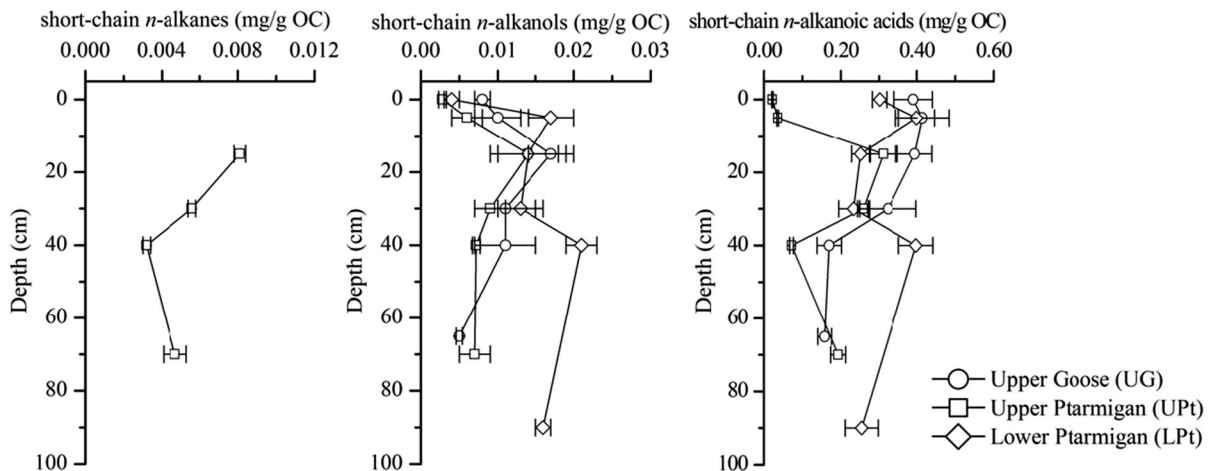
Fig. 4 Concentration of short-chain ($<C_{20}$) acyclic aliphatic lipid concentrations in the soil depth profiles at Cape Bounty. Short-chain *n*-alkanes were not detected in samples from UG and LPt. *Error bars* indicate standard error calculated from triplicate analysis

respectively) while the remaining subsurface soils had *n*-alkanol concentrations ranging from 0.215 ± 0.005 to 0.252 ± 0.004 mg/g OC. The *n*-alkanoic acids observed at the surface of LPt were predominantly long-chain homologues (0.638 ± 0.034 mg/g OC, Fig. 3), though high contributions from short-chain acids (0.301 ± 0.019 mg/g OC, Fig. 4) were also observed. Throughout the subsurface samples, short-chain *n*-alkanoic acids were more abundant (0.233 ± 0.038 to 0.399 ± 0.047 mg/g OC) than the long-chain homologues (0.102 ± 0.006 to 0.164 ± 0.011 mg/g OC). At maximum depth, the LPt soil exhibited comparable quantities of both long-chain (0.214 ± 0.015 mg/g OC) and short-chain (0.254 ± 0.042 mg/g OC) *n*-alkanoic acid constituents. Overall, lower aliphatic lipid concentrations were characteristic throughout the disturbed upslope profile (UPt) and the subsurface soils downslope (LPt). In contrast, higher concentrations of aliphatic lipids were observed in the top 30 cm of the undisturbed soil (UG) surface soil as well as at the surface and the base layer of the disturbed downslope profile (LPt).

The carbon preference index (CPI) for each class of aliphatic lipids (*n*-alkanes, *n*-alkanols, *n*-alkanoic acids) can provide insight into OM diagenesis by comparison of even and odd numbered chain length distributions in lipids which are indicative of source materials. Generally, the CPI proxies produce higher values with the presence of unaltered epicuticular waxes from higher plant-derived material (Eglinton and Hamilton 1967) while values lower than 2 are

characteristic of a more advanced state of degradation (Simoneit 1984; Tuo and Li 2005; Andersson and Meyers 2012). The undisturbed UG profile exhibited relatively high *n*-alkane CPI values, increasing from 4.51 ± 0.31 to 7.10 ± 0.75 in the upper 30 cm and then decreasing from 5.38 ± 0.48 to 2.48 ± 0.44 through the lower portion of the profile (Fig. 5). However, the *n*-alkanol and *n*-alkanoic acid CPI values at UG (Fig. 5) were relatively high throughout the profile suggesting preservation of unaltered OM. Conversely, the *n*-alkane CPI values (Fig. 5) observed throughout the disturbed upslope UPt profile were much lower overall, ranging between 1.17 ± 0.09 to 1.97 ± 0.12. Unlike fresh plant-derived material which generally exhibits a high CPI value, the lower *n*-alkane CPI shown for UPt reflects a more homogenous chain length distribution which is more characteristic of degraded OM (Simoneit 1984; Marzi et al. 1993). Similarly, the *n*-alkanol and *n*-alkanoic acid CPI values at UPt were found to be relatively lower than other sites supporting the presence of altered OM within the upslope disturbed soils (Fig. 5). At the disturbed LPt site, high *n*-alkane CPI values (Fig. 5) from the surface soil (15.6 ± 1.4) and the deepest sample (7.70 ± 1.01) were observed while the other subsurface CPI values ranged between 2.99 ± 0.52 to 3.63 ± 0.50. This suggests the accumulation of unaltered *n*-alkanes at the surface of LPt and potentially indicates the preservation of unaltered material near the base of the active layer (Simoneit and Mazurek 1982; Marzi et al. 1993). Additionally, relatively high
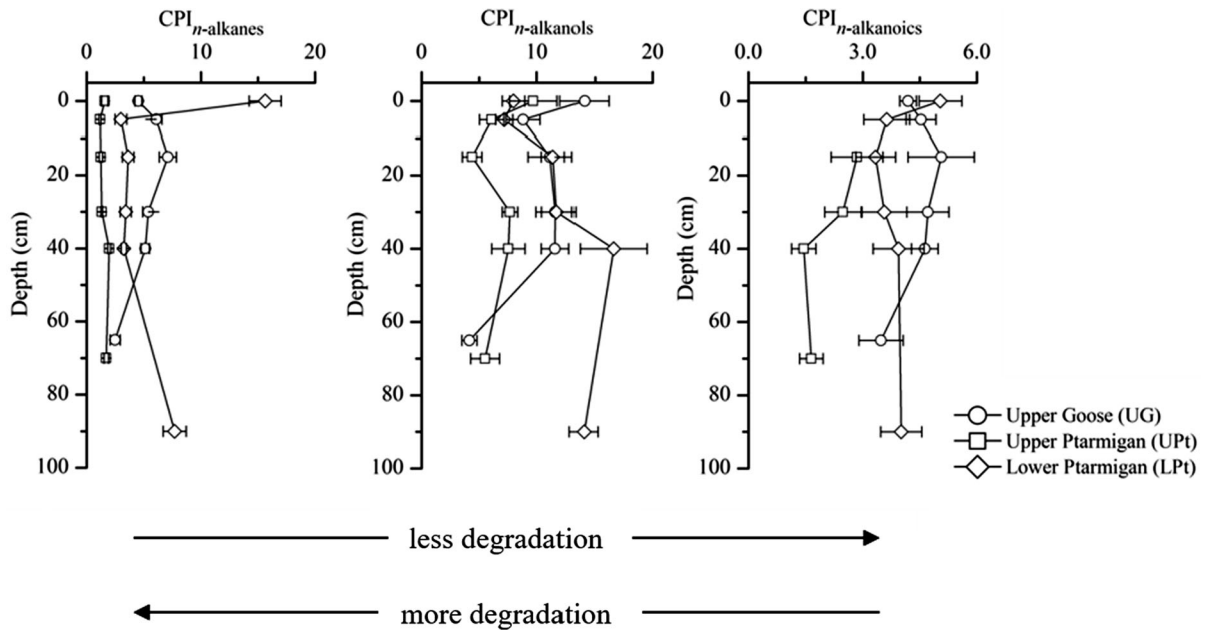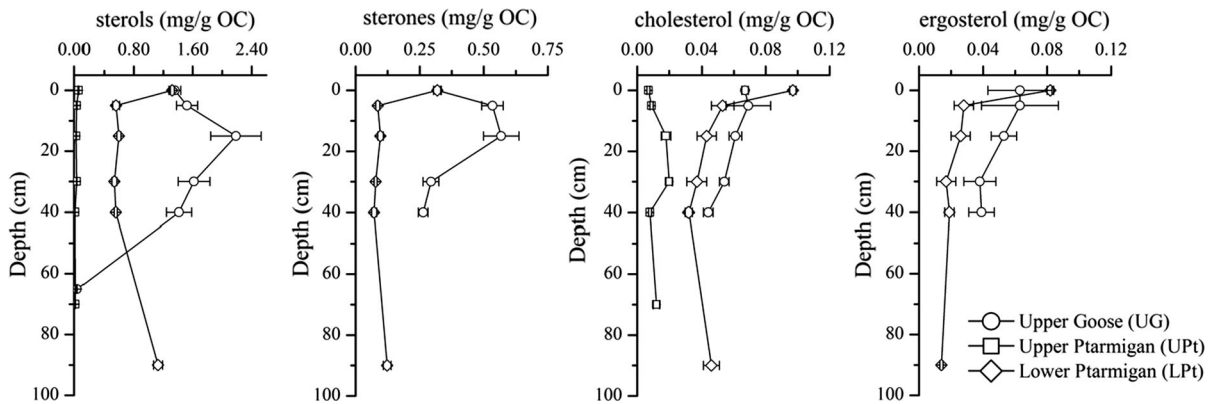
Fig. 5 Carbon preference indices of acyclic aliphatic lipids from soil depth profiles at Cape Bounty. *Error bars* indicate standard error calculated from triplicate analysis. Note: CPI is calculated using carbon chain length ranges of i = 21–33, 20–30, and 20–28 for *n*-alkanes, *n*-alkanols, and *n*-alkanoic acids respectively

CPI values for the *n*-alkanols and *n*-alkanoic acids at LPt were comparable to the undisturbed site indicating the presence of highly unaltered OM throughout the disturbed downslope profile (Fig. 5). Overall, the CPI proxies indicate more advanced OM degradation state within the disturbed upslope soil (UPt) while soils in the disturbed downslope profile appear to be relatively unaltered; particularly within the surface soil and base layer soil at LPt.

The steroids identified in each profile consisted of plant-derived sterols (stigmasterol, campesterol, β-sitosterol, and stigmastanol) and plant-derived sterones (stigmasta-3,5-dien-7-one, sitosterone, and stigmastan-3-one) with minor contributions from cholesterol and ergosterol (Fig. 6). The undisturbed UG profile exhibited the highest concentration of steroids (Fig. 6) with plant-derived sterols ranging from 1.357 ± 0.082 to 2.187 ± 0.342 mg/g OC in the upper 40 cm of the profile while sterones were found in lower concentrations (0.264 ± 0.031 to 0.568 ± 0.069 mg/g OC). Cholesterol (0.044 ± 0.003 to 0.069 ± 0.014 mg/g OC) and ergosterol (0.038 ± 0.010 to 0.063 ± 0.024 mg/g OC) were also observed in the upper 40 cm at UG but in low

concentrations. The soil sampled at maximum depth (65 cm) contained campesterol and β-sitosterol (0.038 ± 0.005 mg/g OC total) but no other steroids were detected. The occurrence of steroids at the disturbed UPt site (Fig. 6) was limited to the plant-derived sterols (0.013 ± 0.001 to 0.060 ± 0.007 mg/g OC) and small concentrations of cholesterol (0.007 ± 0.001 to 0.020 ± 0.002 mg/g OC). Steroids observed at the disturbed LPt profile (Fig. 6) included all those observed in the undisturbed soil (stigmasterol, campesterol, β-sitosterol, stigmastanol, stigmasta-3,5-dien-7-one, sitosterone, stigmastan-3-one, cholesterol, and ergosterol). LPt surface concentrations of these steroids were similar to surface concentrations at the undisturbed site (1.322 ± 0.027, 0.319 ± 0.015, 0.097 ± 0.002, and 0.082 ± 0.002 mg/g OC for plant-derived sterols, plant-derived sterones, cholesterol, and ergosterol respectively). Subsurface LPt soils on the other hand exhibited much lower concentrations of plant-derived sterols (0.537 ± 0.033 to 0.598 ± 0.029 mg/g OC) and sterones (0.072 ± 0.010 to 0.097 ± 0.011 mg/g OC). The range of concentrations for cholesterol and ergosterol at LPt (0.032 ± 0.002 to 0.053 ± 0.007

Fig. 6 Concentration of steroid biomarkers from soil depth profiles at Cape Bounty. *Error bars* indicate standard error calculated from triplicate analysis

and 0.017 ± 0.006 to 0.028 ± 0.006 mg/g OC respectively) were comparable to those at depth in the undisturbed soil (Fig. 6). However, at 90 cm in the LPt profile, the concentration of plant-derived sterols (1.129 ± 0.060 mg/g OC) and sterones (0.123 ± 0.015 mg/g OC) increased while cholesterol (0.046 ± 0.005 mg/g OC) and ergosterol (0.014 ± 0.001 mg/g OC) concentrations remained relatively low. Overall, lower steroid content was observed throughout the disturbed upslope (UPt) soils and subsurface samples in the disturbed downslope profile (LPt). Higher steroid concentrations at the surface and deepest layer of LPt were consistent with the patterns observed with the aliphatic lipids.

The solvent extractable compounds included simple mono- and disaccharides: glucose, mannose, sucrose, and trehalose (Fig. 7). In the undisturbed UG surface soil (0 cm), all four sugars were found at relatively high concentrations (0.595 ± 0.058, 0.583 ± 0.093, 0.791 ± 0.183, and 1.500 ± 0.153 mg/g OC for glucose, mannose, sucrose and trehalose respectively). These sugars were also observed in the disturbed LPt surface soil but lower concentrations of glucose (0.178 ± 0.028 mg/g OC) and mannose (0.194 ± 0.031 mg/g OC) were contrasted by higher concentrations of sucrose (1.109 ± 0.079 mg/g OC) and trehalose (3.381 ± 0.196 mg/g OC). The concentration of all sugars decreased substantially with depth at UG except for trehalose (Fig. 7), which increased in concentration just below the surface (2.257 ± 0.201 mg/g OC, 5–15 cm) before decreasing progressively with depth (1.550 ± 0.150 to 0.007 ± 0.002 mg/g OC, 15–65 cm). In the LPt

subsurface soils (5–90 cm), relatively low concentrations of glucose (0.009 ± 0.002 to 0.019 ± 0.002 mg/g OC), mannose (0.004 ± 0.001 to 0.020 ± 0.002 mg/g OC), and sucrose (0.014 ± 0.004 to 0.122 ± 0.023 mg/g OC) were consistent with the UG soil profile. However, trehalose concentration was lower in the shallowest LPt subsurface soil (0.683 ± 0.096 mg/g OC, 5 cm) and much lower trehalose concentrations were observed at depth (0.052 ± 0.009 to 0.104 ± 0.010 mg/g OC, 15–90 cm) contrasting with the higher trehalose content generally observed in the UG subsurface soils (Fig. 7). Sugars in the disturbed UPt soil profile were nearly absent (Fig. 7) with low concentrations of sucrose and trehalose detected at the surface (0.011 ± 0.003 and 0.123 ± 0.035 mg/g OC respectively) and low concentrations of only trehalose in deeper soils to a maximum depth of 30 cm (0.030 ± 0.004 to 0.018 ± 0.004 mg/g OC). Concentrations of sugars followed a similar trend to that of the aliphatic lipids and steroids with low concentrations throughout the UPt profile and high surface concentrations downslope (LPt). However, sugars within the deepest layer in the disturbed downslope profile (LPt) did not increase as with other biomarkers.

Discussion

Surface soils from the undisturbed UG soil profile have similar properties to those from undisturbed locations within the Ptarmigan region (Pautler et al. 2010a), including: OC % (∼1.4–2.3 %), integrated
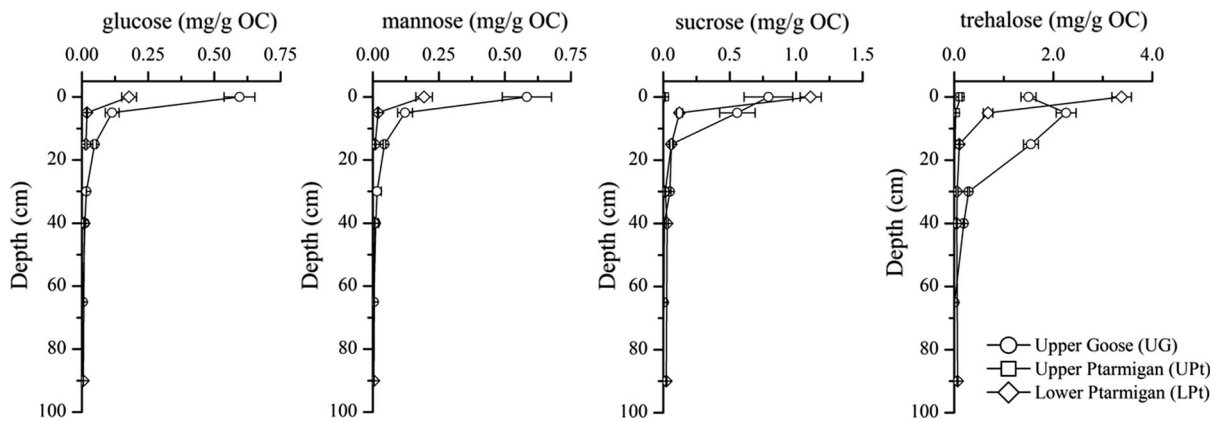
Fig. 7 Concentration of simple sugars from soil depth profiles at Cape Bounty. *Error bars* indicate standard error calculated from triplicate analysis

NMR regions (30–34, 49–51, 11, and 6–8 % for alkyl C, O-alkyl C, aromatic C, and carboxylic C respectively), alkyl/O-alkyl ratios (0.59–0.69) and aliphatic lipid biomarker concentrations (∼0.2–0.4 mg/g OC, ∼1.4 mg/g OC, and ∼0.6–1.3 mg/g OC for *n*-alkanes, *n*-alkanols, and *n*-alkanoic acids respectively). This consistency leads us to suggest that the disturbed UPt soil was also similar prior to the 2007/2008 ALD activity. If this is the case, it appears that the disturbance shifted the established soil profile and transferred material downslope by immediate sliding, leaving exposed clay slurry and ground ice in the upslope scar zone region (Lamoureux and Lafrenière 2009). In addition, the large and sustained increase of suspended sediment observed downstream for several years following the disturbance suggested a redistribution of the exposed soils due to enhanced erosion stimulated by ALD activity (Lewkowicz 2007; Lamoureux and Lafrenière 2009). Throughout the current profile, the disturbed UPt profile exhibited low OC and N content (Table 1), low concentrations of solvent extractable biomarkers (Fig. 3, Table S2), and generally more stable material as suggested by the NMR spectra (Fig. 2b) where low O-alkyl content and a corresponding dominance of aromatic and alkyl C were observed (von Lützow et al. 2006). Comparison of the UPt spectra with that obtained from the deepest undisturbed soil sample (UG, 65 cm) as well as the lowest mid-depth soil from the downslope disturbed site (LPt, 40 cm) reveals a comparable dominance of aromatic and alkyl C (Table 2). These similarities coupled to the mass shift of surface material observed

during the 2007/2008 ALD event indicate that the surface now exposed at UPt scar zone was likely a component of the subsurface mineral soils typically found in High Arctic regions such as Cape Bounty (Ugolini 1986; Goryachkin et al. 1999). The downslope shift of material by the ALD likely removed the pre-existing overlying soil horizons, exposing the current UPt profile to the surface. Additionally, the low *n*-alkane CPI observed throughout UPt (Fig. 5) suggests advanced OM degradation consistent with deeper OM which has been buried over time (Eglinton and Hamilton 1967; Rao et al. 2009). The disturbed profile at UPt lacks substantial O-alkyl content which would be suggestive of such long-term preservation of labile C in the deeper mineral soils. However, the ALD in Ptarmigan constitutes a depression in the landscape which preferentially accumulates wind-blown snow with a hydrological regime characterized by a well-developed network of incised channels enhancing surface erosion during spring runoff and rainfall events (Lamoureux et al. 2014). Recent measurements from the Ptarmigan region also revealed high suspended sediment concentrations while stream water geochemistry from CBAWO confirmed sustained increases to fluvial export of terrestrial-derived material in the region after the disturbance (Lamoureux et al. 2014; Louiseize et al. 2014). Radiocarbon analysis of riverine particulate OM from Ptarmigan suggested the mobilization of aged terrestrial material (6600–6740 years before present) in the disturbed subcatchment (Lamoureux and Lafrenière 2014). Moreover, enhanced lability observed in dissolved

OM (Woods et al. 2011) and fluvial sedimentary OM (Grewer et al. 2015) in the Ptarmigan region downstream of the ALD support the transport of a large amount of labile C from the disturbed soils into the river. With little vegetation to hold the soil, it is likely labile C has been lost to erosion since the ALD events. The increased radiocarbon ages suggest that this exported material may contain previously preserved deep soil C. In addition, degradation in situ and during transport of labile C has been observed with exported soil material hypothesized to originate from Arctic permafrost (Vonk et al. 2010; Spencer et al. 2015) and may also occur in the disturbed UPt soil exposed by the ALDs. Conversely, C loss at the site of the disturbance may potentially occur via microbial degradation of soil OM. However, the concentration of short-chain aliphatic lipids, typically indicative of microbial inputs (Amelung et al. 2008), was low at the surface of UPt (Fig. 4). Hence, microbial consumption likely contributes less to the overall loss of C within the scar zone. Thus, with previous work reporting increased labile C in sedimentary OM downstream (Grewer et al. 2015), fluvial transport mechanisms likely account for greater C losses within the UPt scar zone than microbial degradation.

Downslope in the slump region at LPt, soil was minimally disturbed by ALD activity and hence not subject to enhanced erosion. However, patterned compression ridges were observed in the surface soil produced by the downslope relocation of relatively intact material shifted by the disturbance (Lewkowicz and Harris 2005a; Lamoureux and Lafrenière 2009). High O-alkyl content observed in the surface soil (Fig. 2c) suggests the presence of labile-rich C sources, such as carbohydrates and peptides, while the low alkyl/O-alkyl ratio (Table 2) is consistent with more recently deposited detritus in an early stage of degradation (Baldock and Preston 1995). The early stage of degradation in labile OM implied by the prominent O-alkyl signal is further supported by the relatively high CPI observed in the labile biomarkers (n-alkanols, n-alkanoic acids; Fig. 5). However, a sharp decrease in the O-alkyl content and biomarker concentrations was observed just below the surface of the disturbed LPt soil (Figs. 2c, 3). The shift in OM composition with depth at LPt was not consistent with the distribution in the undisturbed soil at UG. With relatively consistent soil characteristics throughout the region, the downslope profile at Ptarmigan (LPt) likely exhibited similar pre-disturbance OM distributions to the undisturbed soil. However, the pre-existing hydrological network and topography at LPt likely enhanced export of OM during runoff periods prior to the disturbance (Lamoureux et al. 2014) and is consistent with the recalcitrant-rich OM observed in the subsurface soil. At the surface, the formation of lateral compression ridges via the ALD may enhance the retention of post-disturbance runoff material, contributing to the higher OC content observed (Table 1). Hence, comparison with subsurface soil from both the disturbed and undisturbed soils demonstrates a shift at the surface of LPt toward labile-rich OM, likely due to ALD activity. The surface layer also exhibits increased concentrations of long-chain n-alkanes (Fig. 3) and trehalose (Fig. 7). The long-chain n-alkanes, attributed to increased vascular plant input, are generally more persistent than other lipids in soils (Eglinton and Logan 1991; Bush and McInerney 2013). In addition, trehalose, a disaccharide known to be more resistant to decomposition than other simple sugars may be produced by soil microbes in response to freezing and C starvation (Niederer et al. 1992; Silljé et al. 1999; Higashiyama 2002; Shi et al. 2010). These properties suggest that both the n-alkanes and trehalose may preferentially accumulate in Arctic soils over time. The increased concentration of plant-derived n-alkanes and trehalose observed at the surface of the disturbed LPt site and the observed decrease immediately below are indicative of an accumulation of material from the surrounding soil upslope. The observed decrease of O-alkyl content and overall biomarker concentrations in the current subsurface soil may therefore mark the transition between the well-drained pre-ALD profile below, and an agglomeration of the surrounding surface soil retained by the compression ridges above.

Soil OM composition retained by the compression ridges at the surface of the LPt profile exhibit high concentrations of unaltered O-alkyl C at the surface (Fig. 2c). Progressive degradation of the unaltered OM with further warming, accompanied by shifts in microbial populations, may accelerate decomposition and convert the O-alkyl containing species to more accessible forms which may have the potential to increase microbial activity. The long-term outcome of this process results in an overall decline of OM in Arctic and sub-Arctic soils which may be attributed to increased microbial mineralization of C in response to

nutrient and substrate addition, and is referred to as soil priming (Nadelhoffer et al. 1991; Hartley et al. 2010; Lee et al. 2012). Pautler et al. (2010a) observed a surge in microbial activity of surface soils recently disturbed by ALDs at Cape Bounty suggesting the early stages of soil priming. The authors also reported a decrease in labile OM at the site of an historic ALD. In our study, OM distribution in soils from the undisturbed site (UG) was consistent with other undisturbed Arctic soils in the region (Pautler et al. 2010a) exhibiting lower *n*-alkane concentrations and higher concentrations of more labile lipids such as *n*-alkanols and *n*-alkanoic acids in the surface soil (Fig. 3). Conversely, the surface soil at LPt exhibited an enrichment of *n*-alkanes coupled with a decline of labile components such as *n*-alkanols, *n*-alkanoic acids, and simple sugars (Figs. 3, 7). This accumulation of more persistent OM (*n*-alkanes) in addition to reduced levels of labile compounds (*n*-alkanols, *n*-alkanoic acids, and sugars) may result from preferential degradation by microbes, potentially indicating the early stages of priming (von Lützow et al. 2006) and supports results from earlier studies collectively suggesting that priming may contribute to accelerated degradation of OM in High Arctic soils (Hartley et al. 2010; Pautler et al. 2010a). Despite the decreased levels of labile biomarkers, higher O-alkyl content observed via ^{13}C NMR in the surface soil (Table 2) suggests the presence of more complex, unaltered OM such as cellulose which may provide a more sustained C source for microbes. In addition, the compression ridges at LPt may restrict export of OM, prolonging the cycle of growth associated with shifting microbial communities in the context of soil priming (Fontaine et al. 2003). However, the extent to which priming occurs may depend on many other mitigating factors such as the form, concentration, and bioavailability of OM (Kögel-Knabner 2002; Boddy et al. 2008; Kuzyakov 2010), the level ecosystem primary production (Wild et al. 2014), the availability of oxygen, nitrogen, and other crucial nutrients (Sistla et al. 2012; Treat et al. 2015), temperature and moisture content in the soil (Rivkina et al. 2000; Mikan et al. 2002; Boddy et al. 2008), as well as shifting hydrological patterns (Hotchkiss et al. 2014) and export of viable substrate through erosion (Woods et al. 2011; Louiseize et al. 2014). Our study suggests that the formation of compression ridges in the slump region of the ALD promotes accumulation of unaltered OM which may

enhance progressive degradation through soil priming. However, further study of the disturbed soil is necessary to facilitate accurate long-term predictions within different localized environments such as LPt.

With only minor disruption observed near the surface of the downslope region, the deepest LPt soil (90 cm) likely represents older permafrost-derived material being exposed from below the frost table by a thickening active layer. This belowground region near the active layer boundary represents a transition zone where annual fluctuations in climate can potentially alternate the condition of the soil between perennially frozen permafrost and the seasonally thawed active layer over decadal to centennial periods (Shur et al. 2005). As noted previously, OM below the active layer may experience enhanced preservation by perennially freezing within Arctic permafrost, though few studies report the molecular-level composition of these soils (Dutta et al. 2006; Uhlířová et al. 2007; Vonk and Gustafsson 2013). While relatively high summer temperature recorded from 2007 at CBAWO was considered to be instrumental in the initiation of ALDs (Lamoureux and Lafrenière 2009), warmer than average temperatures during the year of sampling (Favaro and Lamoureux 2014) strongly suggest that the 2012 active layer depth observed at LPt represents much deeper thawing than is typically observed (Lamoureux et al. 2014). Accordingly, the high concentration of labile lipids (*n*-alkanols and *n*-alkanoic acids, Fig. 3) and the prominent O-alkyl resonance observed in the NMR spectrum (Fig. 2c) support the presence of labile OM deep within the LPt profile which may imply the release of labile permafrost-derived OM from below the frost table upon active layer thickening. Within the O-alkyl region of the NMR spectrum (90+ cm; Fig. 2c), the most intense peak (65–95 ppm) corresponds with oxygen substituted C, ring C in carbohydrates, and C from ether groups. In addition, the prominent anomeric C signal (105 ppm) suggests that the O-alkyl C content observed at depth likely contains a relatively large proportion of carbohydrates. However, the low concentrations of extractable sugars observed (Fig. 7) suggest the presence of more complex carbohydrates such as cellulose, likely preserved by the low temperatures and greater moisture retention in the LPt soil resulting from accumulated snow cover in the downslope region extending the seasonal melting period. In contrast, a lack of labile C observed within the deeper

upslope soil (UPt) exposed by the ALD suggests that the preservation of OM in permafrost below the active layer may not be uniform throughout the soils of CBAWO. With minimal disruption at LPt however, the labile OM observed at depth likely corresponds to the release of OM preserved below the active layer, providing an example of the OM composition potentially stored at the transition zone between the active layer and continuous permafrost in Canadian High Arctic soils.

Conclusion

This study found that OM content and character is altered by ALDs in Canadian High Arctic soils with surface horizons of the disturbed regions experiencing the most marked shift in OM composition. Many studies of Arctic soil have reported the preservation of labile OM below the active layer (Sjögersten et al. 2003; Zimov et al. 2006b; Waldrop et al. 2010; Vonk and Gustafsson 2013; Schuur et al. 2015), yet our results indicate the removal of the overlying soils by ALDs in the upslope region exposed mineral soils with low concentrations of labile OM. However, given the potential enhancement of fluvial export via surface runoff erosion and previous work confirming the accumulation of labile C downstream of the ALD, it is likely that much of the OM from the disturbed upslope site would have been mobilized downstream. In the downslope slump region, the formation of compression ridges at the surface disrupted the well-established pre-ALD hydrological network, likely enhancing the accumulation of OM. Deep below the surface in the downslope region, increased active layer thickness revealed an enrichment of labile C at depth likely a result of long-term preservation in permafrost. Results from our study thus demonstrate how ALDs may alter soil OM composition with depth and to varying extents between the upslope and downslope regions of the detachment. However, slope variability across the landscape was not studied directly and hence conclusions regarding the shift of pre-ALD OM composition from upslope or downslope areas are limited. Examination of the spatial heterogeneity in ALD-impacted areas should therefore be the focus of future work to determine the scale of compositional shifts in soil OM imposed by ALD activity. Additionally, continued disruption over future freeze–thaw

cycles may heighten erosion during spring-thaw runoff, increasing terrestrial-derived inputs to the surrounding aquatic systems (Wang and Bettany 1993; Schimel and Clein 1996; Henry 2007). Hence, further monitoring of disturbed areas such as CBAWO is necessary to provide an increasingly accurate assessment of potential shifts in biogeochemical cycling in the High Arctic.

References

Amelung W, Brodowski S, Sandhage-Hofmann A, Bol R (2008) Combining biomarker with stable isotope analyses for assessing the transformation and turnover of soil organic matter. Adv Agron 100:155–250

Andersson RA, Meyers PA (2012) Effect of climate change on delivery and degradation of lipid biomarkers in a Holocene peat sequence in the Eastern European Russian Arctic. Org Geochem 53:63–72

Baldock JA, Preston CM (1995) Chemistry of carbon decomposition processes in forests as revealed by solid-state carbon-13 nuclear magnetic resonance. In: McFee WW, Kelly JM (eds) Carbon forms and functions in forest soils. Soil Sci Soc Am, Madison, pp 89–117

Bockheim JG, Tarnocai C (1998) Recognition of cryoturbation for classifying permafrost-affected soils. Geoderma 81:281–293

Boddy E, Roberts P, Hill PW, Farrar J, Jones DL (2008) Turnover of low molecular weight dissolved organic C (DOC) and microbial C exhibit different temperature sensitivities in Arctic tundra soils. Soil Biol Biochem 40:1557–1566

Bowden WB, Gooseff MN, Malser A, Green A, Peterson BJ, Bradford J (2008) Sediment and nutrient delivery from thermokarst features in the foothills of the North Slope, Alaska: potential impacts on headwater stream ecosystems. J Geophys Res 113:G02026

Bush RT, McInerney FA (2013) Leaf wax *n*-alkane distributions in and across modern plants: implications for paleoecology and chemotaxonomy. Geochim Cosmochim Ac 117:161–179

Conte P, Spaccini R, Piccolo A (2004) State of the art of CPMAS 13C-NMR spectroscopy applied to natural organic matter. Prog Nucl Magn Reson Spectrosc 44:215–223

Davidson EA, Janssens IA (2006) Temperature sensitivity of soil carbon decomposition and feedbacks to climate change. Nature 440:165–173

Davis N (2001) Permafrost: a guide to frozen ground in transition. Fairbanks, Alaska

Dinel H, Schnitzer M, Mehuys GR (1990) Soil lipids: origin, nature, content, decomposition, and effect on soil physical properties. In: Bollag JM, Stotzky G (eds) Soil Biochemistry. Marcel Dekker, New York, pp 397–427

Drake TW, Wickland KP, Spencer RGM, McKnight DM, Striegl RG (2015) Ancient low-molecular-weight organic acids in permafrost fuel rapid carbon dioxide production upon thaw. Proc Natl Acad Sci USA 112:13946–13951

Dria KJ, Sachleben JR, Hatcher PG (2002) Solid-state carbon-13 nuclear magnetic resonance of humic acids at high magnetic field strengths. J Environ Qual 31:393–401

Dutta K, Schuur EAG, Neff JC, Zimov SA (2006) Potential carbon release from permafrost soils of Northeastern Siberia. Global Chang Biol 12:2336–2351

Eglinton G, Hamilton RJ (1967) Leaf epicuticular waxes. Science 156:1322–1335

Eglinton G, Logan G (1991) Molecular Preservation. Philos Trans R Soc B 333:315–328

Ewing SA, Donnell JAO, Aiken GR, Butler K, Butman D, Windham-Myers L, Kanevskiy MZ (2015a) Long-term anoxia and release of ancient, labile carbon upon thaw of Pleistocene permafrost. Geophys Res Lett 42:10730–10738

Ewing SA, Paces JB, O'Donnell JA, Jorgenson MT, Kanevskiy MZ, Aiken GR, Shur YL, Harden JW, Striegl RG (2015b) Uranium isotopes and dissolved organic carbon in loess permafrost: modeling the age of ancient ice. Geochim Cosmochim Acta 152:143–165

Favaro EA, Lamoureux SF (2014) Antecedent controls on rainfall runoff response and sediment transport in a High Arctic catchment. Geogr Ann B 96:433–446

Fontaine S, Mariotti A, Abbadie L (2003) The priming effect of organic matter: a question of microbial competition? Soil Biol Biochem 35:837–843

Fontaine S, Bardoux G, Abbadie L, Mariotti A (2004) Carbon input to soil may decrease soil carbon content. Ecol Lett 7:314–320

Goryachkin SV, Karavaeva NA, Targulian VO, Glazov MV (1999) Arctic soils: spatial distribution, zonality and transformation due to global change. Permafrost Periglac 10:235–250

Grewer DM, Lafrenière MJ, Lamoureux SF, Simpson MJ (2015) Potential shifts in Canadian High Arctic sedimentary organic matter composition with permafrost active layer detachments. Org Geochem 79:1–13

Hartley IP, Hopkins DW, Sommerkorn M, Wookey PA (2010) The response of organic matter mineralisation to nutrient and substrate additions in sub-arctic soils. Soil Biol Biochem 42:92–100

Harwood JL, Russell NJ (1984) Lipids in plants and microbes. George Allen and Unwin, London

Henry HAL (2007) Soil freeze-thaw cycle experiments: trends, methodological weaknesses and suggested improvements. Soil Biol Biochem 39:977–986

Higashiyama T (2002) Novel functions and applications of trehalose. Pure Appl Chem 74:1263–1269

Hobbie SE, Nadelhoffer KJ, Hogberg P (2002) A synthesis: the role of nutrients as constraints on carbon balances in boreal and arctic regions. Plant Soil 242:163–170

Hodgson DA, Vincent JS, Fyles JG (1984) Quaternary geology of Central Melville Island, Northwest Territories. Geol Surv Can Pap 83–16:1–25

Hotchkiss ER, Hall RO, Baker MA, Rosi-Marshall EJ, Tank JL (2014) Modeling priming effects on microbial consumption of dissolved organic carbon in rivers. J Geophys Res Biogeosci 119:982–995

Johns TJ, Angove MJ, Wilkens S (2015) Measuring soil organic carbon: which technique and where to from here? Soil Res 53:717–736

Jorgenson MT, Shur YL, Pullman ER (2006) Abrupt increase in permafrost degradation in Arctic Alaska. Geophys Res Lett 33:L02503

Kögel-Knabner I (1997) ^{13}C and ^{15}N NMR spectroscopy as a tool in soil organic matter studies. Geoderma 80:243–270

Kögel-Knabner I (2002) The macromolecular organic composition of plant and microbial residues as inputs to soil organic matter. Soil Biol Biochem 34:139–162

Koven CD, Ringeval B, Friedlingstein P, Ciais P, Cadule P, Khvorostyanov D, Krinner G, Tarnocai C (2011) Permafrost carbon-climate feedbacks accelerate global warming. P Natl Acad Sci USA 108:14769–14774

Kuzyakov Y (2002) Review: factors affecting rhizosphere priming effects. J Plant Nutr Soil Sc 165:382–396

Kuzyakov Y (2010) Priming effects: interactions between living and dead organic matter. Soil Biol Biochem 42:1363–1371

Lamoureux SF, Lafrenière MJ (2009) Fluvial impact of extensive active layer detachments, Cape Bounty, Melville Island, Canada. Arct Antarct Alp Res 41:59–68

Lamoureux SF, Lafrenière MJ (2014) Seasonal fluxes and age of particulate organic carbon exported from Arctic catchments impacted by localized permafrost slope disturbances. Environ Res Lett 9:045002

Lamoureux SF, Lafrenière MJ, Favaro EA (2014) Erosion dynamics following localized permafrost slope disturbances. Geophys Res Lett 41:5499–5505

Lantz TC, Kokelj SV (2008) Increasing rates of retrogressive thaw slump activity in the Mackenzie Delta region, NWT, Canada. Geophys Res Lett 35:L06502

Lee H, Schuur EAG, Inglett KS, Lavoie M, Chanton JP (2012) The rate of permafrost carbon release under aerobic and anaerobic conditions and its potential effects on climate. Global Chang Biol 18:515–527

Lewis T, Braun C, Hardy DR, Francus P, Bradley RS (2005) An extreme sediment transfer event in a Canadian High Arctic stream. Arct Antarct Alp Res 37:477–482

Lewis T, Lafrenière MJ, Lamoureux SF (2012) Hydrochemical and sedimentary responses of paired High Arctic watersheds to unusual climate and permafrost disturbance, Cape Bounty, Melville Island, Canada. Hydrol Process 26:2003–2018

Lewkowicz AG (2007) Dynamics of active-layer detachment failures, Fosheim Peninsula, Ellesmere Island, Nunavut, Canada. Permafrost Periglac 18:89–103

Lewkowicz AG, Harris C (2005a) Morphology and geotechnique of active-layer detachment failures in discontinuous and continuous permafrost, northern Canada. Geomorphology 69:275–297

Lewkowicz AG, Harris C (2005b) Frequency and magnitude of active-layer detachment failures in discontinuous and continuous permafrost, Northern Canada. Permafrost Periglac 69:275–297

Louiseize NL, Lafrenière MJ, Hastings MG (2014) Stable isotopic evidence of enhanced export of microbially derived NO_3^- following active layer slope disturbance in the Canadian High Arctic. Biogeochemistry 121:565–580

MacDougall AH, Avis CA, Weaver AJ (2012) Significant contribution to climate warming from the permafrost carbon feedback. Nat Geosci 5:719–721

Mann PJ, Eglinton TI, McIntyre CP, Zimov N, Davydova A, Vonk JE, Holmes RM, Spencer RGM (2015) Utilization of ancient permafrost carbon in headwaters of Arctic fluvial networks. Nat Commun 6:7856

Marzi R, Torkelson BE, Olson RK (1993) A revised carbon preference index. Org Geochem 20:1303–1306

Mikan CJ, Schimel JP, Doyle AP (2002) Temperature controls of microbial respiration in arctic tundra soils above and below freezing. Soil Biol Biochem 34:1785–1795

Nadelhoffer K, Giblin A, Shaver G, Laundre J (1991) Effects of temperature and substrate quality on element mineralization in 6 Arctic Soils. Ecology 72:242–253

Natali SM, Schuur EAG, Webb EE, Pries CEH, Crummer KG (2014) Permafrost degradation stimulates carbon loss from experimentally warmed tundra. Ecology 95:602–608

Nelson DW, Sommers LE (1996) Total carbon, organic carbon, and organic matter. In: Sparks DL (ed) Methods of soil analysis. Part 3: Chemical methods. Soil Science Society of America, Inc., American Society of Agronomy, Inc., Madison, Wisconsin, USA, pp 961–1010

Niederer M, Pankow W, Wiemken A (1992) Seasonal changes of soluble carbohydrates in mycorrhizas of Norway spruce and changes induced by exposure to frost and desiccation. Eur J Forest Pathol 22:291–299

Nowinski NS, Trumbore SE, Schuur EAG, Mack MC, Shaver GR (2008) Nutrient addition prompts rapid destabilization of organic matter in an arctic tundra ecosystem. Ecosystems 11:16–25

Otto A, Simpson MJ (2005) Degradation and preservation of vascular plant-derived biomarkers in grassland and forest soils from Western Canada. Biogeochemistry 74:377–409

Pautler BG, Simpson AJ, Mcnally DJ, Lamoureux SF, Simpson MJ (2010a) Arctic permafrost active layer detachments stimulate microbial activity and degradation of soil organic matter. Environ Sci Technol 44:4076–4082

Pautler BG, Austin J, Otto A, Stewart K, Lamoureux SF, Simpson MJ (2010b) Biomarker assessment of organic matter sources and degradation in Canadian High Arctic littoral sediments. Biogeochemistry 100:75–87

Preston CM (2014) Environmental NMR: solid-state methods. In: Simpson MJ, Simpson AJ (eds) NMR spectroscopy: a versatile tool for environmental research. Wiley, New York

Preston C, Trofymow J, Sayer B, Niu J (1997) C-13 nuclear magnetic resonance spectroscopy with cross-polarization and magic-angle spinning investigation of the proximate-analysis fractions used to assess litter quality in decomposition studies. Can J Bot 75:1601–1613

Rao Z, Zhu Z, Wang S, Jia G, Qiang M, Wu Y (2009) CPI values of terrestrial higher plant-derived long-chain n-alkanes: a potential paleoclimatic proxy. Front Earth Sci 3:266–272

Rivkina E, Friedmann E, McKay C, Gilichinsky D (2000) Metabolic activity of permafrost bacteria below the freezing point. Appl Environ Microb 66:3230–3233

Rumpel C, Rabia N, Derenne S, Quenea K, Eusterhues K, Kögel-Knabner I, Mariotti A (2006) Alteration of soil organic matter following treatment with hydrofluoric acid (HF). Org Geochem 37:1437–1451

Rutherford PM, McGill WB, Arocena JM, Figueiredo CT (2008) Total nitrogen. In: Carter MR, Gregorich EG (eds) Soil sampling and methods of analysis, 2nd edn. Taylor and Francis Group, Boca Raton, pp 239–250

Schaefer K, Zhang T, Bruhwiler L, Barrett AP (2011) Amount and timing of permafrost carbon release in response to climate warming. Tellus B 63:165–180

Schimel JP, Clein JS (1996) Microbial response to freeze–thaw cycles in tundra and taiga soils. Soil Biol Biochem 28:1061–1066

Schuur EAG, Vogel JG, Crummer KG, Lee H, Sickman JO, Osterkamp TE (2009) The effect of permafrost thaw on old carbon release and net carbon exchange from tundra. Nature 459:556–559

Schuur EAG, McGuire AD, Schädel C, Grosse G, Harden JW, Hayes DJ, Hugelius G, Koven CD, Kuhry P, Lawrence DM, Natali SM, Olefeldt D, Romanovsky VE, Schaefer K, Turetsky MR, Treat CC, Vonk JE (2015) Climate change and the permafrost carbon feedback. Nature 520:171–179

Shi L, Sutter BM, Ye X, Tu BP (2010) Trehalose is a key determinant of the quiescent metabolic state that fuels cell cycle progression upon return to growth. Mol Biol Cell 21:1982–1990

Shur Y, Hinkel KM, Nelson FE (2005) The transient layer: implications for geocryology and climate-change science. Permafrost Periglac 16:5–17

Silljé HHW, Paalman JWG, ter Schure EG, Olsthoorn SQB, Verkleij AJ, Boonstra J, Verrips CT (1999) Function of trehalose and glycogen in cell cycle progression and cell viability in *Sacchromyces cerevisiae*. J Bacteriol 181:396–400

Simoneit B (1984) Organic-matter of the troposphere. 3. Characterization and sources of petroleum and pyrogenic residues in aerosols over the Western United-States. Atmos Environ 18:51–67

Simoneit BRT, Mazurek MA (1982) Organic matter of the troposphere. 2. Natural background of biogenic lipid matter in aerosols over the rural western United States. Atmos Environ 16:2139–2159

Simpson MJ, Otto A, Feng X (2008) Comparison of solid-state carbon-13 nuclear magnetic resonance and organic matter biomarkers for assessing soil organic matter degradation. Soil Sci Soc Am J 72:268–276

Sistla SA, Shinichi A, Schimel JP (2012) Detecting microbial N-limitation in tussock tundra soil: implications for Arctic soil organic carbon cycling. Soil Biol Biochem 55:78–84

Sjögersten S, Turner BL, Mahieu N, Condron LM, Wookey PA (2003) Soil organic matter biochemistry and potential susceptibility to climatic change across the forest-tundra ecotone in the Fennoscandian mountains. Global Chang Biol 9:759–772

Spencer RGM, Mann PJ, Dittmar T, Eglinton TI, McIntyre C, Holmes RM, Zimov N, Stubbins A (2015) Detecting the signature of permafrost thaw in Arctic rivers. Geophys Res Lett 42:2830–2835

Tarnocai C, Canadell JG, Schuur EAG, Kuhry P, Mazhitova G, Zimov S (2009) Soil organic carbon pools in the northern

circumpolar permafrost region. Glob Biogeochem Cycles 23:GB2023

Treat CC, Natali SM, Ernakovich J, Iversen CM, Lupascu M, McGuire AD, Norby RJ, Chowdhury TR, Richter A, Šantrůčková H, Schadel C, Schuur EAG, Sloan VL, Turetsky MR, Waldrop MP (2015) A pan-Arctic synthesis of CH_4 and CO_2 production from anoxic soil incubations. Glob Chang Biol 21:2787–2803

Tuo JC, Li Q (2005) Occurrence and distribution of long-chain acyclic ketones in immature coals. Appl Geochem 20:553–568

Ugolini FC (1986) Peodgenic zonation in the well-drained soils of the Arctic regions. Quat Res 26:100–120

Uhlířová E, Šantrůčková H, Davidov SP (2007) Quality and potential biodegradability of soil organic matter preserved in permafrost of Siberian tussock tundra. Soil Biol Biochem 39:1978–1989

von Lützow M, Kögel-Knabner I, Ekschmitt K, Matzner E, Guggenberger G, Marschner B, Flessa H (2006) Stabilization of organic matter in temperate soils: mechanisms and their relevance under different soil conditions—a review. Eur J Soil Sci 57:426–445

Vonk JE, Gustafsson O (2013) Permafrost-carbon complexities. Nat Geosci 6:675–676

Vonk JE, van Dongen BE, Gustafsson Ö (2010) Selective preservation of old organic carbon fluvially released from sub-Arctic soils. Geophys Res Lett 37:L11605

Waldrop MP, Wickland KP, White R III, Berhe AA, Harden JW, Romanovsky VE (2010) Molecular investigations into a globally important carbon pool: permafrost-protected carbon in Alaskan soils. Glob Chang Biol 16:2543–2554

Walker DA, Raynolds MK, Daniels FJA, Einarsson E, Elvebakk A, Gould WA, Katenin AE, Kholod SS, Markon CJ, Melnikov ES, Moskalenko NG, Talbot SS, Yurtsev BA (2005) The circumpolar Arctic vegetation map. J Veg Sci 16:267–282

Wang FL, Bettany JR (1993) Influence of freeze–thaw and flooding on the loss of soluble organic-carbon and carbon-dioxide from soil. J Environ Qual 22:709–714

Wild B, Schnecker J, Alves RJE, Barsukov P, Barta J, Capek P, Gentsch N, Gittel A, Guggenberger G, Lashchinskiy N, Mikutta R, Rusalimova O, Santruckova H, Shibistova O, Urich T, Watzka M, Zrazhevskaya G, Richter A (2014) Input of easily available organic C and N stimulates microbial decomposition of soil organic matter in arctic permafrost soil. Soil Biol Biochem 75:143–151

Woods GC, Simpson MJ, Pautler BG, Lamoureux SF, Lafrenière MJ, Simpson AJ (2011) Evidence for the enhanced lability of dissolved organic matter following permafrost slope disturbance in the Canadian High Arctic. Geochim Cosmochim Acta 75:7226–7241

Zimov S, Schuur E, Chapin F (2006a) Permafrost and the global carbon budget. Science 312:1612–1613

Zimov SA, Davydov SP, Zimova GM, Davydova AI, Schuur EAG, Dutta K, Chapin FS (2006b) Permafrost carbon: stock and decomposability of a globally significant carbon pool. Geophys Res Lett 33:L20502